Contrib Mineral Petrol (2004) 147: 276–287
DOI 10.1007/s00410-004-0557-3

ORIGINAL PAPER

Werner Schreyer · Heinz-Jürgen Bernhardt
André-Mathieu Fransolet · Thomas Armbruster

# End-member ferrian kanonaite: an andalusite phase with one Al fully replaced by (Mn, Fe)$^{3+}$ in a quartz vein from the Ardennes mountains, Belgium, and its origin

Received: 1 September 2003 / Accepted: 19 December 2003 / Published online: 25 February 2004


**Abstract** Kanonaite, with compositions plotting on the join $Mn^{3+}AlSiO_5$–$Fe^{3+}AlSiO_5$, was discovered in a late quartz vein of the Le Coreux metamorphic manganese deposit. A typical structural formula is $(Mn^{3+}_{3.69}Fe^{3+}_{0.36})Al_{3.95}Si_{4.00}O_{20}$, representing maximum solid solution within the system $Al_2SiO_5$–$Mn_2SiO_5$–$Fe_2SiO_5$. Refractive indices are $\beta' = 1.777$; $\gamma' = 1.855$. The end-member compositions form the outermost, latest products in zoned crystals ranging to less manganiferous kanonaite. A crystal structure determination of a Mn-rich kanonaite confirms that about 96% of all the $Mn^{3+}$ present is located in the strongly Jahn-Teller-distorted octahedron of the andalusite-type structure. Combining all relevant mineral-chemical and petrological data available on the deposit, a speculative model is presented in which kanonaite crystals with successively higher $Mn^{3+}$ contents form during decreasing temperatures in the course of the anticlockwise PTt path of extensional metamorphism. Kaolinite occurring in zones within composite kanonaite porphyroblasts of adjacent phyllites is regarded here as by-product of a continuous retrograde breakdown reaction of less manganiferous kanonaite. In places, kanonaite was peripherally replaced by muscovite and Mn- and Fe-oxides.

Dedicated to the late Dr. H.S. Yoder, Jr.

Editorial responsibility: J. Hoefs

W. Schreyer (✉) · H.-J. Bernhardt
Institut für Geologie, Mineralogie und Geophysik,
Ruhr-Universität, 44780 Bochum, Germany
E-mail: werner.schreyer@ruhr-uni-bochum.de
Tel.: +49-234-32 23522
Fax: +49-234-32 14433

A.-M. Fransolet
Institut de Minéralogie, Université de Liège, Bâtiment B 18,
Sart Tilman, 4000 Liège, Belgium

T. Armbruster
Laboratorium für chemische und mineralogische Kristallographie,
University of Bern, Freiestr. 3, 3012 Bern, Switzerland

## Introduction

Among the aluminium silicates, $Al_2SiO_5$, andalusite is distinctive in that one Al per formula unit is in the unusual fivefold coordination with oxygen, while the other Al occupies a strongly distorted octahedron (Burnham and Buerger 1961). The structural formula of andalusite may be written as $^{[6]}Al^{[5]}AlO[SiO_4]$. The tetragonally distorted octahedral site preferably accommodates cations such as trivalent manganese which, due to their electronic configuration, may become similarly distorted upon entering the structure (Jahn-Teller effect). With the partial substitution of $^{[6]}Al$ by $Mn^{3+}$, andalusite develops spectacular green colours and pleochroism, which were the reason for the initial name "viridine" (Klemm 1911).

In the early 1980s the Commission on New Minerals and Mineral Names (CNMMN) of the International Mineralogical Association (IMA) voted to abandon the mineral name "viridine" used for Mn-bearing andalusites (for details see Gunter and Bloss 1982), because a particularly $Mn^{3+}$-rich andalusite had been discovered in nature, which allowed the definition of an end member. According to Vrána et al. (1978), it contains more $Mn^{3+}$ (76 atom%) in the octahedral site than Al. The new mineral was named kanonaite after the type locality in Zambia and given the formula $^{[6]}Mn^{3+}{}^{[5]}AlO[SiO_4]$. However, following the rules of IMA-CNMMN for mineral solid solutions, it may contain up to 50 mol% of $Al_2SiO_5$ (aluminian kanonaites). Consequently, former "viridines" containing more than 50 mol% of $Al_2SiO_5$ are now called manganian andalusites (Fig. 1).

Experimental studies by Abs-Wurmbach et al. (1983a) revealed that $Mn^{3+}$ incorporation drastically stabilizes the andalusite structure relative to those of sillimanite and kyanite, i.e. both towards higher temperatures and higher pressures. In addition, $Mn^{3+}$-bearing andalusite phases become stable by dehydration reactions involving hydrous Al-silicates such as

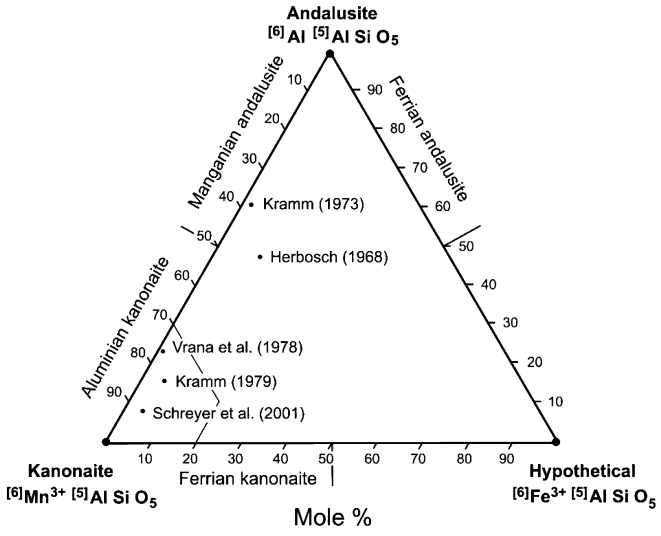


**Fig. 1** Ternary plot of the system $Al_2SiO_5$–$MnAlSiO_5$–"$FeAlSiO_5$" showing minerals characterized by the andalusite structure and their nomenclature. Manganian andalusite replaced the abandoned name "viridine". *Dots* indicate natural mineral compositions reported by the authors indicated. Note that those of Kramm (1979) and Schreyer et al. (2001) refer only to the most manganiferous members out of their respective analyses. The *framed area* near the kanonaite end member is shown in an enlarged version in Fig. 4

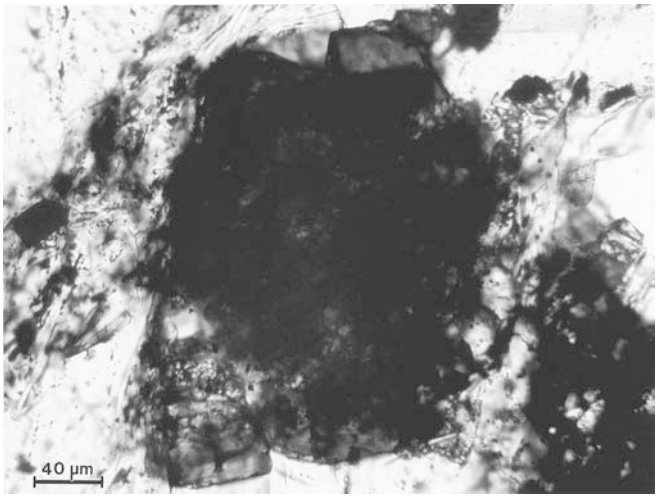


**Fig. 2** Transmitted-light photograph of largely opaque kanonaite aggregate (*centre*) in sample Cor 8-1. Only towards the rims (*top*, *lower left*, *right*) can some small transparent kanonaite crystals be recognized. Along its *upper left edge*, the opaque kanonaite is surrounded by an elongated aggregate of small flakes of muscovite and additional opaques

kaolinite and pyrophyllite at considerably lower temperatures than pure andalusite in the system $Al_2O_3$–$SiO_2$–$H_2O$. These same authors also found that the degree of $^{[6]}Al$ replacement by $Mn^{3+}$ at temperatures above about 500 °C is limited to the range of manganian andalusites (Fig. 1), whereas Mn-richer kanonaites could only be synthesized at lower temperatures. Thus, the fully Mn-substituted kanonaite end member, if it exists, can only be expected at very low temperatures.

Following the kanonaite discovery by Vrána et al. (1978), Kramm (1979) analysed the former "viridine" crystals of the classic locality Le Coreux in the Belgian Ardennes, and found them to be chemically zoned with compositions extending beyond the 50 mol% limit into the kanonaite field (Fig. 1). The outermost rims of the porphyroblasts analysed attain about 79 mol% kanonaite end member and are considered to have formed under retrograde metamorphic conditions (Kramm 1979). From late quartz veins of the same locality, Schreyer et al. (2001) described kanonaites containing up to 88 mol% $Mn^{3+}AlSiO_5$ end member, the balance being largely $Al_2SiO_5$ and some "$Fe^{3+}AlSiO_5$" (Fig. 1).

In the present paper, we report on truly extreme kanonaite compositions from another quartz vein sample of the same locality. Octahedral Al is calculated to be nil, whereas the sums of $Mn^{3+}$ and $Fe^{3+}$ are equal to, or even slightly exceed unity. The spatial relationships of these end-member ferrian kanonaites to Mn-poorer ones in the same sample allow cautious conclusions concerning the PTX-stability relations of kanonaite.

## Geology and petrography

The outcrop of Le Coreux, about 1 km north of Salmchâteau, is located in the south-eastern part of the Stavelot Massif, a Caledonian basement inlier near the north-western border of the Hercynian Rhenish Massif in the Belgian Ardennes. Within the Ordovician metasedimentary sequence which underwent low-grade metamorphism during late Hercynian times, an about 10-m-thick conformable horizon of deep-purple phyllites confines the classical mineral locality. The former pelites were unusually rich in highly oxidized manganese and gave rise during metamorphism to a wealth of manganese minerals. They are particularly enriched within late quartz veins and have been studied for over a century. Note that the outcrop is of very limited extent, so that no variations of metamorphic grade and history can be expected. Following the classical descriptions, the regional and local geology and mineralogy were summarized by Fransolet et al. (1977), Kramm (1982) and Schreyer et al. (2001).

The present study focuses on the mineralogy of a particular quartz vein which, unfortunately, was only found as a loose boulder of about 8-cm diameter (sample Cor 8). Quartz, by far the dominant mineral, forms interlocking, strongly strained grains up to 1 cm across. Locally along grain boundaries, annealing recrystallization into finer-grained crystal fabrics with foam structure can be observed. Some portions of the sample contain large isolated crystals of albite with inclusions of muscovite. There is less than 5% of opaque, or opaque-appearing minerals, among which is kanonaite (Fig. 2). Together with some muscovite, these opaques form very thin, subparallel, discontinuous layers, which are often isoclinally folded between and within the large quartz

grains. Typical needles and whiskers of the newly found hollandite-type mineral (Schreyer et al. 2001) occur rarely in some of the layers. Blocky braunite is more common but difficult to distinguish (in transmitted light) from opaque-appearing kanonaite crystals also displaying rectangular outlines. Another common opaque mineral is hematite, often directly adjacent to kanonaite or, together with braunite, occurring as small to minute inclusions within kanonaite. Reflected-light and electron microprobe work revealed also some grains of intergrown Mn-oxide/hydroxide phases (according to analytical data, probably pyrolusite replacing manganite; see Ramdohr 1980, Fig. 589b), which are confined to late alteration zones surrounding kanonaite. Therefore, they are not considered to be part of a primary excess-Mn assemblage with kanonaite. Frequently, these thin-skinned alteration zones also contain well-oriented flakes of muscovite and fine-grained hematite (Fig. 2). Muscovite orientation follows the subparallel layering in the vein and probably defines a weak late schistosity.

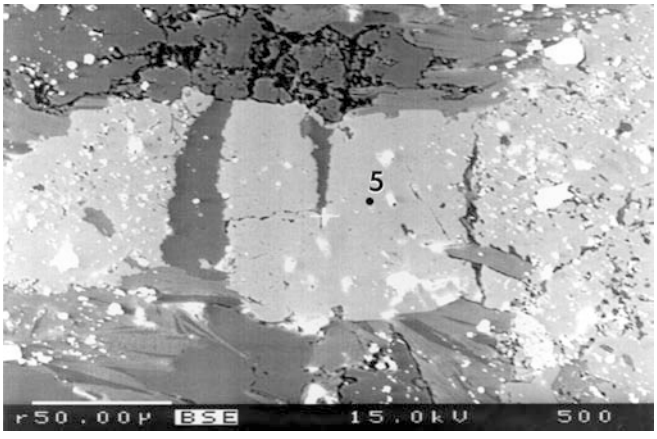


**Fig. 3** Backscattered electron (BSE) image of anhedral (*left* and *right*) as well as partly euhedral crystals of kanonaite (grey, *centre*) surrounded by quartz and muscovite. Whereas the kanonaite crystals on the *left* and *right* contain multitudes of small to minute bright inclusions of braunite and hematite, those in the *centre* are nearly free of them. In transmitted light, the latter are transparent, displaying strong "viridine" pleochroism (from *green* to *brown*), while the former ones appear opaque (compare Fig. 2). The central transparent crystal was used for structure analysis. Point 5 is the location of the electron microprobe analysis listed in Table 1 with the same number. Sample Cor 8-1

The opaque-appearing kanonaite crystals which, for this reason, can easily be overlooked in thin section are occasionally transparent along their edges (Fig. 2), and display unusually intense pleochroism ranging from very dark emerald-green to dark coffee-brown. Moreover, the optical relief appears to be higher than for the kanonaite occurrences known previously. This was confirmed by reflectivity measurements reported below. Optical observations at high magnification, both in transmitted and reflected light, revealed that the overall opaque nature of most of the kanonaite is due to the presence of numerous minute opaque inclusions of hematite and braunite which are best seen in backscattered electron (BSE) images (Fig. 3).

## Kanonaite compositions

Electron microprobe analyses were performed on four polished thin sections of sample Cor 8 at Ruhr-University Bochum, using the same instrument and identical operating conditions as reported by Schreyer et al. (2001). BSE imaging following careful reflected-light studies as well as some 150 reconnaissance semiquantitative energy dispersive (EDS) spectra revealed that the kanonaite crystals show considerable chemical variations both within and among single crystals. Thirty-four quantitative analyses were performed on individual spots within crystals. A selection of ten analyses is presented in Table 1, arranged in the order of decreasing

**Table 1** Selected microprobe analyses of kanonaite from Le Coreux (sample Cor 8)

| | 1 | 2 | 3 | 4 | 5 | 6 | 7 | 8 | 9 | 10 |
|---|---|---|---|---|---|---|---|---|---|---|
| $SiO_2$ | 31.73 | 31.29 | 31.04 | 31.63 | 31.45 | 31.23 | 31.41 | 31.59 | 31.84 | 32.33 |
| $TiO_2$ | 0.00 | 0.03 | 0.05 | 0.01 | 0.03 | 0.03 | 0.00 | 0.02 | 0.00 | 0.01 |
| $Al_2O_3$ | 26.56 | 27.02 | 27.18 | 26.91 | 27.15 | 26.74 | 27.01 | 26.75 | 28.98 | 32.33 |
| $Fe_2O_3$ | 3.79 | 3.12 | 3.08 | 3.58 | 3.44 | 3.43 | 3.74 | 4.47 | 3.48 | 3.17 |
| $Mn_2O_3$ | 38.28 | 38.27 | 38.11 | 38.09 | 38.04 | 38.00 | 37.92 | 37.27 | 36.26 | 31.88 |
| MgO | 0.04 | 0.01 | 0.03 | 0.02 | 0.03 | 0.03 | 0.01 | 0.02 | 0.03 | 0.02 |
| CaO | 0.05 | 0.00 | 0.00 | 0.01 | 0.02 | 0.00 | 0.00 | 0.03 | 0.00 | 0.03 |
| Total | 100.46 | 99.74 | 99.49 | 100.24 | 100.16 | 99.46 | 100.09 | 100.15 | 100.59 | 99.77 |
| Based on 20 oxygens | | | | | | | | | | |
| $Si^{4+}$ | 4.004 | 3.970 | 3.948 | 3.995 | 3.974 | 3.976 | 3.973 | 3.996 | 3.974 | 3.996 |
| $^{[4]}Al^{3+}$ | | 0.030 | 0.052 | 0.005 | 0.026 | 0.024 | 0.027 | 0.004 | 0.026 | 0.004 |
| $^{[5]}Al^{3+}$ | 3.951 | 4.000 | 4.000 | 4.000 | 4.000 | 3.989 | 4.000 | 3.983 | 4.000 | 4.000 |
| $^{[6]}Al^{3+}$ | | 0.011 | 0.023 | - | 0.017 | - | - | - | 0.236 | 0.706 |
| $Fe^{3+}$ | 0.360 | 0.298 | 0.295 | 0.340 | 0.327 | 0.329 | 0.356 | 0.425 | 0.327 | 0.295 |
| $Mn^{3+}$ | 3.677 | 3.696 | 3.690 | 3.661 | 3.658 | 3.683 | 3.651 | 3.588 | 3.445 | 2.999 |
| Ti | 0.000 | 0.003 | 0.005 | 0.001 | 0.003 | 0.003 | 0.000 | 0.002 | 0.000 | 0.001 |
| Mg | 0.008 | 0.002 | 0.006 | 0.003 | 0.005 | 0.006 | 0.002 | 0.003 | 0.005 | 0.003 |
| Ca | 0.007 | 0.000 | 0.000 | 0.001 | 0.003 | 0.000 | 0.000 | 0.005 | 0.000 | 0.004 |
| Σ | 4.052 | 4.010 | 4.019 | 4.006 | 4.013 | 4.021 | 4.009 | 4.023 | 4.013 | 4.008 |
| Σcat | 12.007 | 12.010 | 12.019 | 12.006 | 12.013 | 12.010 | 12.009 | 12.006 | 12.013 | 12.008 |

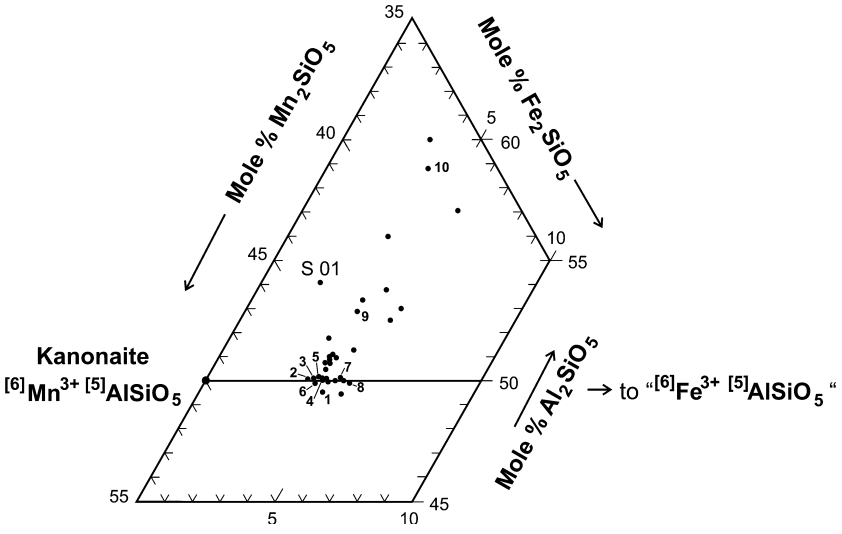


**Fig. 4** Enlarged portion of the extended system $Al_2SiO_5$–"$Mn_2SiO_5$–$Fe_2SiO_5$" with its upper portion being identical to the *framed area* of Fig. 1. However, this plot uses different end-member components, so that the numbers of mol% given here are half of those shown in Fig. 1. *Dots* indicate the chemical compositions of kanonaite analysed in sample Cor 8 except for S 01, which is the previously Mn-richest kanonaite composition (Schreyer et al. 2001). The *small numbers* refer to the analyses listed in Table 1. Some compositions plot slightly below the baseline $MnAlSiO_5$–"$FeAlSiO_5$" of Fig. 1, indicating a small surplus of $(Mn+Fe)^{3+}$ over the theoretical 1:1 ratio to Al

Mn, but with highly manganiferous ones dominating. All Mn and Fe is calculated to be trivalent. In addition to the other major elements Si and Al, only minor amounts of Ti, Mg and Ca were found which will be neglected in the discussions to follow.

The analytical data are normalized to an oxygen basis of 20 in Table 1. This leads to Si values mostly somewhat below the ideal 4.0 per formula unit (p.f.u.), so that small amounts of Al are attributed to the tetrahedral site. The remaining Al is, except for analyses nos. 9–10, just about sufficient to fill the five-coordinated site. Thus, in these cases, there are no, or only trifling amounts of Al left to be attributed to the six-coordinated site, which is essentially occupied by Mn and Fe. This displays, at least in the calculation, the end-member character of the kanonaite analyses 1–8.

All 34 kanonaite analyses are plotted in Fig. 4 in the relevant portion of Fig. 1 near the ideal kanonaite end member—however, somewhat expanded towards still less aluminous compositions. The most manganiferous analyses, e.g. nos. 1–8 of Table 1, plot very closely to the join $Mn^{3+}AlSiO_5$–"$Fe^{3+}AlSiO_5$", whereas many others spread into the ternary field with $Al_2SiO_5$ contents much beyond the thus far least aluminous kanonaite S 01 of Schreyer et al. (2001). Note that some analyses (e.g. no. 1 of Table 1) even plot below the tie line $MnAlSiO_5$–"$FeAlSiO_5$". Although it is possible that these deviations are due to analytical uncertainties, there is no a-priori reason that the baseline of Fig. 1 indeed represents the limit of kanonaite solid solution. The crystal structure determination by Weiss et al. (1981) of the holotype kanonaite of Vrána et al. (1978; see Fig. 1 here) had shown that only about 86 atom% of all the $Mn^{3+}$ present occupies the octahedral site, whereas the remaining 14% resides in the five-coordinated position. If so, the absolute end member of the manganese solid solution series could actually be $Mn_2SiO_5$, as indicated in Fig. 4. Bearing in mind, however, that the kanonaites analysed here coexist with excess Mn-oxide phases (see above), they are likely to represent maximum Mn contents for the conditions of their crystallization. Thus, at least from a bulk chemical point of view, the most manganiferous kanonaite analyses plotting along the join $MnAlSiO_5$–"$FeAlSiO_5$" of Fig. 4 do seem to represent end-member compositions.

Similar arguments hold for the ferric iron contents of the kanonaites analysed, because hematite is an excess phase in the quartz vein and provides $Fe^{3+}$ saturation. Therefore, the ideal Fe-free kanonaite end member $MnAlSiO_5$ cannot be attained, rather only about 92 mol% of it (=46 mol% of $Mn_2SiO_5$ in Fig. 4). The $Fe_2SiO_5$ component in the 34 kanonaite analyses of sample Cor 8 varies between about 3 and 6 mol% (Fig. 4), equalling about 6 to 12 mol% "$FeAlSiO_5$", the latter value being among the highest measured worldwide. More extreme values, such as 28 mol% determined by wet chemical analysis in "viridines" from the Aldan Shield, Siberia (Kulish 1961), seem to be erroneous, because the more recent microprobe analyses on samples from this same locality resulted in only 10–12 mol% "$FeAlSiO_5$" (Abs-Wurmbach et al. 1981).

A major problem poses, of course, the considerable chemical variation of the kanonaite analysed here (Table 1), which occurs between as well as within single crystals. In the latter case, microscopic and mineral analytical observations can provide a clue for the time sequence of these variations. The BSE image of Fig. 5 exhibits irregular kanonaite zoning, where the subhedral, apparently corroded prism consists largely of light (Mn-rich) portions which include and replace darker

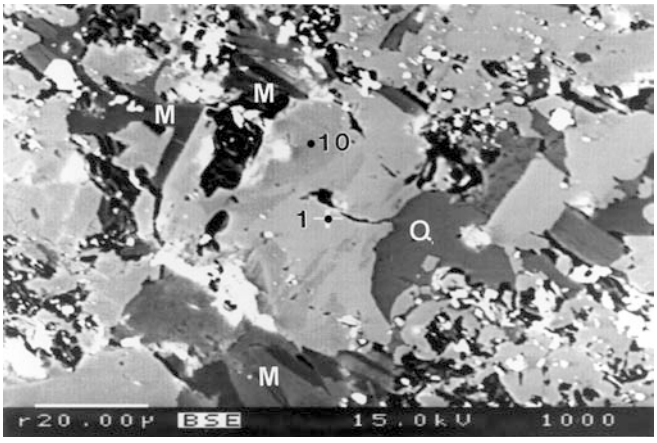


**Fig. 5** BSE image of kanonaite (*grey*) surrounded by quartz (*Q*), muscovite (*M*) and bright Mn- and Fe-oxides. The kanonaite crystal in the *centre* is chemically heterogeneous, consisting of *darker grey*, Mn-poor (mainly on *left side*) and *lighter grey*, Mn-richer portions. Some of these include small patches of the darker kanonaite. Points 1 and 10 indicate the locations of the requisite EMP analyses in Table 1. Note signs of corrosion along the *left side* of the formerly perhaps euhedral kanonaite crystal where it abuts against muscovite being part of the latest alteration assemblage. Sample Cor 8-1

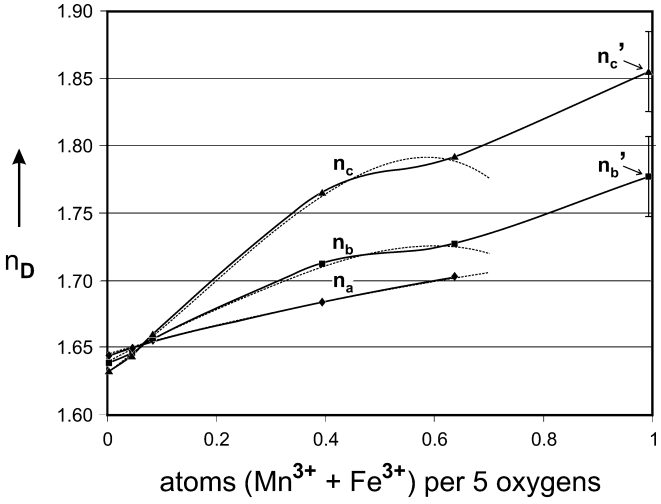


**Fig. 6** Plot of refractive indices of minerals in the andalusite–kanonaite system versus contents of total ($Mn^{3+} + Fe^{3+}$) after Gunter and Bloss (1982). The data at ($Mn^{3+} + Fe^{3+}$) near 1 were calculated from measured reflectances of a crystal of the end-member ferrian kanonaite described here (see text). For the sake of clarity, many data points of Gunter and Bloss (1982) at low (Mn, Fe) were omitted, but their curves given up to ($Mn^{3+} + Fe^{3+}$) = 0.7 are reproduced as *dashed lines*. Note that the new data points at ($Mn^{3+} + Fe^{3+}$) near 1 do not lie on any extension of these curves. Error bars ±0.03 as discussed in the text. *Solid lines* merely connect points; $n_b$, etc., indicate refractive index in the direction of crystallographic b, $n_b$' one close to this direction

(Mn-poorer) parts. The mutual boundaries are very sharp. Spots 1 and 10 were analysed, and their compositions are given by these numbers in Table 1. They differ in their $Mn_2O_3$ contents by more than 6 wt% and plot at extreme positions in Fig. 4. We conclude from these and similar observations that the end-member ferrian kanonaites of sample Cor 8 represent the later products of crystallization relative to their Mn-poorer companions.

## Optical properties of end-member ferrian kanonaite

Due to the very high optical relief and strong colouring of the end-member ferrian kanonaite, its refractive indices could not be measured directly by conventional methods. Therefore, the specular reflectances in air and in immersion oil were determined at 589 nm for two loosely defined directions within the crystal. According to the pleochroic absorption formula given by Gunter and Bloss (1982), these two directions are close to those of crystallographic b (very dark emerald-green) and c (dark coffee-brown). On the basis of the measured values, refractive indices were calculated using the two-media method (see Piller 1977, p. 135). Experience with this method shows that its maximum error is in the order of 0.03. The values obtained are 1.777 for $n_b$' (= $\beta$') and 1.855 for $n_c$' (= $\gamma$'). These refractive indices were plotted in Fig. 6, using the diagram with previous data presented by Gunter and Bloss (1982) as well as their symbols. It can be seen that the values for the end-member ferrian kanonaite described here lie along more or less linear extrapolation trends of the curves for $n_b$ and $n_c$ as given by Gunter and Bloss (1982, Fig. 3) who, on the other hand, had introduced curvatures towards lower values with increasing ($Mn^{3+} + Fe^{3+}$) in the kanonaite range (see Fig. 6). Our new data do not support such curvatures. Gunter and Bloss (1982) had emphasized that "$Mn^{3+}$ increases the refractive indices less effectively than $Fe^{3+}$", so that deviations from linearity may be caused by variable Mn/Fe ratios. The variations in Mn/Fe observed for our end-member crystals (Table 1 and Fig. 4) cannot explain the curvature assumed by Gunter and Bloss (1982).

## Crystal structure

The schematic structure of kanonaite (Fig. 7) shows the strongly elongated axial vector O4–$Mn^{3+}$–O4 due to Jahn-Teller distortion of the cation. The trans–trans edge-sharing octahedral chains parallel to the *c* axis have the Jahn-Teller elongation direction perpendicular to the chains and resemble the octahedral chains in manganite, $Mn^{3+}OOH$ (Hoffmann et al. 1997, their Fig. 3a).

The aim of the single-crystal structure study is (1) to characterize a close to end-member kanonaite of ideal composition $MnAlO[SiO_4]$, and (2) to evaluate the possible distribution of $Mn^{3+}$ among the octahedral and five-coordinated site, as suggested by Weiss et al. (1981). The relatively inclusion-free crystal containing point 5 in Fig. 3 and Table 1 was removed from the thin section and used for X-ray data collection. It was

entirely immersed in glue so that its exact size in the third dimension could not be evaluated. Data collection and refinement details are given in Table 2. X-ray

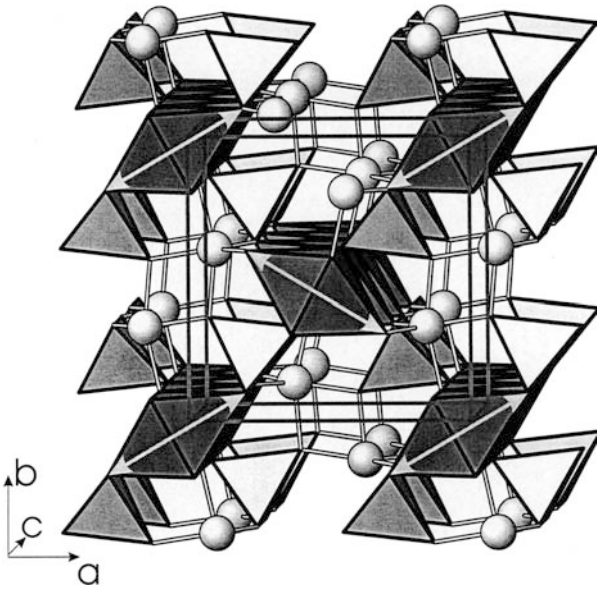


**Fig. 7** Polyhedral drawing of the structure of kanonaite. Jahn-Teller elongated $Mn^{3+}$ octahedra (*light arrows* indicate the direction of elongation) form edge-sharing chains parallel to the *c* axis. Al (spheres with bonds) prefers distorted trigonal bipyramidal coordination forming edge-sharing dimers

**Table 2** CCD data collection and refinement of kanonaite

| | |
|---|---|
| Diffractometer | Siemens SMART CCD system |
| X-ray radiation | Sealed tube MoK$\alpha$ |
| X-ray power | 50 kV, 40 mA |
| Temperature | 293 K |
| Detector to sample distance | 5.2 cm |
| Detector 2 theta angle | 27° |
| Rotation axis | $\omega$ |
| Rotation width | 0.3° |
| Total number of frames | 1,271 |
| Frame size | 512×512 pixels |
| Data collection time per frame | 60 s |
| Collection mode | Hemisphere |
| Reflections measured | 1,710 |
| Max. $2\theta$ | 54.6; $-8 \le h \le 10$, $-10 \le k \le 9$, $-6 \le l \le 7$ |
| Unique reflections | 432 |
| Reflections > $2\sigma$(I) | 329 |
| Space group | *Pnnm* (no. 58) |
| Cell dimensions | $a = 8.001(3), b = 8.101(3), c = 5.629(2), V = 364.9(4)$ Å$^3$ |
| R(int) | 6.4% |
| R($\sigma$) | 5.0% |
| Number of l.s. parameters | 47 |
| GooF | 0.986 |
| R1, Fo > 4$\sigma$(Fo) | 3.24% |
| R1, all data | 5.76% |
| wR2 (on $F^2$)[a] | 6.00% |

[a] $R1 = (\sum ||F_o| - |F_c||)/(\sum |F_o|)$,

$wR2 = \sqrt{\left(\sum \left(F_o^2 - F_c^2\right)^2\right) \Big/ \left(\sum w\left(F_o^2\right)^2\right)}$,

$GooF = \sqrt{\left(\sum w\left(F_o^2 - F_c^2\right)^2\right) \Big/ (n-p)}$

scattering factors for Fe and Mn are too similar, and thus these elements cannot be distinguished in diffraction experiments using MoK$\alpha$ X-radiation. Therefore, Mn scattering factors were used to model Mn and minor Fe. The refinement was performed with the program SHELX97 (Sheldrick 1997), allowing for anisotropic displacement parameters for all atoms and refining Mn/Al occupancy for Mn1 (octahedron) and Al2 (trigonal bipyramid). Atomic coordinates, anisotropic displacement parameters and selected bond lengths are given in Tables 3, 4 and 5. In addition, a test refinement has been performed with the chemical composition constrained to $MnAlO[SiO_4]$, in agreement with analysis no. 5 in Table 1. However, this refinement converged at significantly higher agreement factor and was abandoned.

The structurally refined formula is $(Mn, Fe)_{0.88}Al_{1.12}SiO_5$. At first glance, this seems to be in disagreement with the electron microprobe analysis of point 5 (Table 1) for which the composition $Mn_{0.90}Fe_{0.08}Al_{1.02}SiO_5$ was analysed. However, there are two possibilities to consider:

1. Most end-member kanonaite crystals of sample Cor 8 have been found to be zoned with respect to Al and (Mn, Fe), as shown in Fig. 5. Electron microprobe analyses of a crystal appearing homogeneous in two dimensions cannot exclude that the crystal is actually zoned in the third dimension (perpendicular to the analysed area).
2. There is also some ambiguity in the diffraction experiments if the data are not collected to high diffraction angles, which was unsuitable for our sample due to the small crystal size. In particular, for low-resolution diffraction data, the scale factor exhibits a strong inverse correlation with the refined occupancy of the heaviest atoms. However, this effect was tested with a refinement constrained to the analysed chemistry.

Trivalent manganese displays a strong preference (Table 3) for octahedral coordination and exhibits characteristic, tetragonally elongated (4 + 2) Jahn-Teller distortion (Table 5), in agreement with earlier results on

**Table 3** Atomic coordinates and isotropic displacement parameter $U_{equi}$of kanonaite, space group *Pnnm* (no. 58), $a = 8.001(3)$, $b = 8.101(3)$, $c = 5.629(2)$ Å, $V = 364.9(4)$ Å$^3$

| Atom | x/*a* | y/*b* | z/*c* | $U_{equi}$ |
|---|---|---|---|---|
| Mn1[a] | 0.00000 | 0.00000 | 0.24279(14) | 0.0082(3) |
| Al2[b] | −0.12452(18) | 0.36351(17) | 0.00000 | 0.0073(5) |
| Si | 0.2504(2) | 0.25580(18) | 0.00000 | 0.0097(4) |
| O1 | 0.0735(4) | −0.1369(4) | 0.00000 | 0.0119(8) |
| O2 | 0.4244(4) | 0.3628(4) | 0.00000 | 0.0114(8) |
| O3 | 0.1042(5) | 0.3987(4) | 0.00000 | 0.0129(8) |
| O4 | 0.2461(3) | 0.1437(3) | 0.2375(4) | 0.0117(6) |

[a] Mn1 (octahedron) is occupied by 0.842(4) Mn + Fe and 0.158(4) Al

[b] Al2 (five-coordinated) is occupied by 0.962(4) Al and 0.038(4) (Mn + Fe)

**Table 4** Anisotropic displacement parameters of kanonaite

| Atom | $U_{11}$ | $U_{22}$ | $U_{33}$ | $U_{23}$ | $U_{13}$ | $U_{12}$ |
|---|---|---|---|---|---|---|
| Mn1 | 0.0103(4) | 0.0062(4) | 0.0079(4) | 0.00000 | 0.00000 | 0.0017(4) |
| Al2 | 0.0070(8) | 0.0064(7) | 0.0085(7) | 0.00000 | 0.00000 | −0.0001(7) |
| Si | 0.0102(7) | 0.0067(7) | 0.0123(7) | 0.00000 | 0.00000 | 0.0002(5) |
| O1 | 0.014(2) | 0.009(2) | 0.013(2) | 0.00000 | 0.00000 | 0.004(2) |
| O2 | 0.013(2) | 0.010(2) | 0.011(2) | 0.00000 | 0.00000 | −0.001(2) |
| O3 | 0.013(2) | 0.010(2) | 0.016(2) | 0.00000 | 0.00000 | −0.001(2) |
| O4 | 0.014(1) | 0.009(1) | 0.012(1) | 0.001(1) | −0.0011(9) | −0.001(1) |

**Table 5** Selected bond lengths for kanonaite (values in *italics* from Weiss et al. 1981 and Abs-Wurmbach et al. 1981)

| | This study | Weiss et al. | Abs-Wurmbach et al. |
|---|---|---|---|
| Mn1–O1 (2x) | 1.856(3) | *1.850* | *1.853* |
| Mn1–O2 (2x) | 1.923(3) | *1.916* | *1.918* |
| Mn1–O4 (2x) | 2.288(2) | *2.244* | *2.245* |
| Mean | 2.022 | *2.003* | *2.005* |
| Al2–O4 (2x) | 1.805(2) | *1.806* | *1.803* |
| Al2–O3 | 1.853(4) | *1.849* | *1.856* |
| Al2–O3′ | 1.933(4) | *1.923* | *1.926* |
| Al2–O1 | 1.880(4) | *1.864* | *1.860* |
| Mean | 1.855 | *1.850* | *1.850* |
| Si–O4 (2x) | 1.616(2) | *1.621* | *1.624* |
| Si–O2 | 1.641(4) | *1.641* | *1.639* |
| Si–O3 | 1.646(4) | *1.635* | *1.636* |
| Mean | 1.630 | *1.630* | *1.631* |

Mn-poorer crystals (Abs-Wurmbach et al. 1981; Weiss et al. 1981). A good measure of the tetragonal distortion is the disproportionate increase of the Mn1–O4 distance compared to the remaining M1–O distances with increasing Mn content (Table 5). In the crystal analysed by us, as much as about 96% of the total (Mn + Fe) is ordered in Mn1, rather than 86% as found by Weiss et al. (1981). This supports the suggestion that the join kanonaite–"$FeAlSiO_5$" represents the limit of ternary solid solutions for andalusite-type structures in the system $Al_2SiO_5$–"$Mn_2SiO_5$"–"$Fe_2SiO_5$" (Fig. 4). The distorted trigonal bipyramid of Al2 (five-coordinated site) in kanonaite is not suited for significant incorporation of ions with $3d^4$ high-spin configuration. In contrast, a five-coordinated square pyramidal site, as observed in vesuvianite, is ideal for $Mn^{3+}$ incorporation (e.g. Armbruster and Gnos 2000). This suggests that the minor concentration of 0.038(4) (Mn, Fe) p.f.u. refined on the bipyramidal site in kanonaite is mainly $Fe^{3+}$. This assumption is also in good agreement with Mössbauer data (Abs-Wurmbach et al. 1981) indicating that ca. 10–15% of the total $Fe^{3+}$ in kanonaite is positioned on the bipyramdial Al site. Abs-Wurmbach et al. (1981) assumed that in their kanonaite structure refinement all Fe and Mn is positioned on the octahedral site, and fixed the occupancy of the bipyramidal site for Al = 1. Notice that kanonaite from the type locality studied by Abs-Wurmbach et al. (1981) had only 0.018 $Fe^{3+}$ p.f.u. Thus, 10–15% of this content are below the traceability of the diffraction experiment, but can be resolved by Mössbauer spectroscopy.

In order to verify the structurally determined (Mn + Fe) concentration, the unit cell volumes of manganian andalusites and aluminous kanonaites of Gunter and Bloss (1982) were plotted versus (Mn + Fe) p.f.u. (Fig. 8). A linear regression analysis yielded a volume of 369.2 Å$^3$ for the theoretical end member $MnAlSiO_5$. The smaller cell volume and the refined (Mn + Fe) of the investigated crystal plot close to the extrapolated regression line. In addition, good agreement with the regression line is found for the data on natural samples studied by Abs-Wurmbach et al. (1981). Only the kanonaite investigated by Weiss et al. (1981) displays strong deviation from the predicted trend. This may be due to an incorrect chemical composition assumed by these authors from their structure determination. The three chemical analyses published by Vrána et al. (1978), Abs-Wurmbach et al. (1981), and Gunter and Bloss (1982) on kanonaite samples from the type locality show considerably lower Mn contents than that given by Weiss et al. (1981). In addition, the fact that Mn differs in these three analyses over a range of nearly 7 wt% $Mn_2O_3$ indicates considerable chemical variations among samples from the type locality. Most importantly, Weiss et al. (1981) did not analyse the composition of the crystal applied for structure analysis but derived the chemical formula from site occupancy refinements. Thus, the inverse correlation between scale factor and occupancy has also to be considered for their data. It is interesting to note that the kanonaite crystal (from the same locality) studied by Abs-Wurmbach et al. (1981) with the analysed composition $Mn_{0.680}Fe_{0.018}Al_{1.302}O[SiO_4]$ has the same unit cell volume as the crystal structurally investigated by Weiss et al. (1981), and even the average bond lengths of the two structural studies are not significantly different (Table 5). From this evidence we may assume that the chemical compositions of these two specimens are also very similar.

## Changing chemistry of the Le Coreux andalusite–kanonaite minerals and its possible origins

With the discovery of end-member ferrian kanonaite in the quartz vein described here, the full range of replacement of octahedral Al in andalusite by ($Mn^{3+}$, $Fe^{3+}$) from 0 to 100% is now established for the Le Coreux locality and its direct metapelitic country rock. This is also a novelty worldwide! Genetic reasons for this astonishing variability could be (1) that the availability of excess manganese and iron in the fluid forming the quartz vein changed in time and space, and (2) that—provided freely reacting ($Mn^{3+}$, $Fe^{3+}$) were always and everywhere available—the maximum extent of solid solution in the andalusite–kanonaite system varied with the changing conditions of pressure, temperature and oxygen fugacity during vein formation. These reasons may also apply to occurrences within the phyllites.

For a discussion of this alternative, we review here first the existing knowledge on the occurrence of these

minerals within the phyllitic country rock at Le Coreux, where they form macroscopically visible, dark inclusion-rich porphyroblasts (Herbosch 1968; Kramm 1973, 1979). Surprisingly, Kramm (1979) found that these porphyroblasts are compositionally inhomogeneous, showing strong zonations from about 50 mol% $MnAlSiO_5$ in their cores to the maximum value of 79 mol% along their rims (Fig. 1), and explained this feature by a late Mn pulse due to retrograde unmixing of Mn from coexisting hematite in the rock. This notion would imply that the Mn-poorer cores were formed at a time when no reactive excess Mn was available. At any rate, Kramm (1979) linked the Mn increase of kanonaite porphyroblasts during their growth with decreasing temperatures of metamorphism. Strangely enough, he also recognized porphyroblasts with intermediate zones of kaolinite, which he interpreted as alteration products of former pure andalusite.

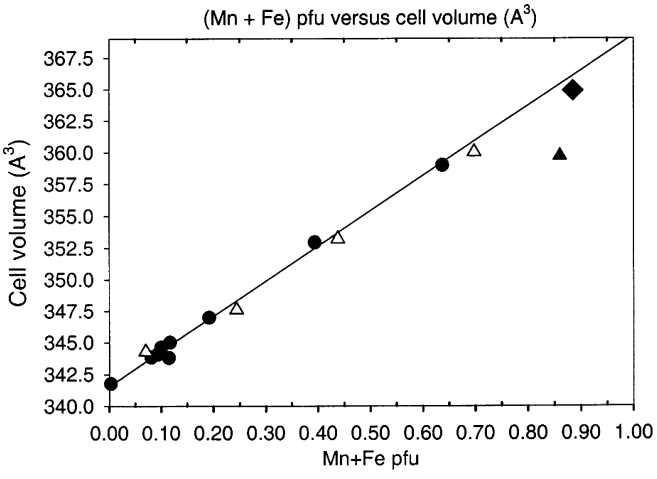


**Fig. 8** Dependence of the unit cell volume of manganian andalusites (formerly "viridines") and aluminous kanonaites on the degree of $(Mn, Fe)^{3+}$ substitution for Al. *Filled circles* and *regression line* Gunter and Bloss (1982), *open triangles* Abs-Wurmbach et al. (1981), *filled triangle* Weiss et al. (1981), *filled diamond* this study. Standard deviations of all data are smaller than the size of the symbols (*pfu* atoms per formula unit based on five oxygens). For a discussion of the deviating Weiss et al. (1981) result, see text

The fundamental question as to whether or not the andalusite–kanonaite minerals at Le Coreux were saturated with (Mn, Fe) throughout their history of formation can be approached by studying their parageneses in the thin sections. Table 6 lists a selection of cases in which andalusite–kanonaite of a particular composition coexists with other, excess-(Mn, Fe)-bearing minerals. Because of the varying valences of Mn and of additional components present in these minerals, complications arise which can only be touched upon here. The presence of tetravalent Mn in hollandite, $(Ba, Sr)Mn^{3+}{}_2Mn^{4+}{}_6O_{16}$, seems to indicate sufficiently high degrees of oxidation, but the necessary presence of Ba and Sr in the fluid may also be of influence. On the other hand, braunite, $Mn^{2+}Mn^{3+}{}_6O_8SiO_4$, carries divalent Mn and would seem to indicate somewhat lower oxidation. However, as shown experimentally by Abs-Wurmbach et al. (1983b) and Abs-Wurmbach and Peters (1999), braunite is stable up to the very high oxygen fugacities of the $Mn_2O_3/MnO_2$ buffer. Still more importantly for the present problem, Abs-Wurmbach and Peters (1999) defined the phase relations in the system Mn–Al–Si–O as a function of varying oxygen fugacities. Although their results only apply to the fixed PT condition of 4 kbar, 600 °C—thus implying that the maximum Mn content of their andalusite/kanonaite phase is only in the range of manganian andalusite (Fig. 1; see below)—this limiting composition coexists, for the conditions of the $Mn_2O_3/MnO_2$ buffer, with braunite + quartz. This assemblage is identical to the Mn-buffering assemblage as observed at Le Coreux (Table 6). Therefore, it can be concluded that the various mole percentages $MnAlSiO_5$ as given in Table 6 do represent stable limiting compositions for particular conditions of pressure and temperature at high oxygen fugacities. Note, however, that braunite + quartz does not define a particular oxygen fugacity.

Concerning the component $FeAlSiO_5$ in the andalusite/kanonaites of Le Coreux (Table 6), the additional presence of hematite + quartz defines a limiting Fe content. This is not the case for the kanonaite described by Schreyer et al. (2001), and explains its decidedly lower Fe contents than that reported here (Table 6). Local Fe deficiencies may also apply to the relatively Fe-poor kanonaite crystals of sample Cor 8 (Fig. 4).

**Table 6** Extreme compositions and related buffering assemblages of andalusite–kanonaite minerals from Le Coreux

| Reference | Composition (mol%) | | Buffering assemblage (no oxygen buffer)[a] | Remarks |
|---|---|---|---|---|
| | $MnAlSiO_5$ | $FeAlSiO_5$ | | |
| Kramm (1973) | 37.6 | 1.8 | Braun + hem + qtz | Porphyroblast |
| Kramm (1979) | 79.0 | 5.9 | Braun + hem + qtz | Zoned porphyroblast |
| Schreyer et al. (2001) | 87.5 | 4.1 | Braun + qtz only, hol | In quartz vein |
| This paper | 89.2 | 10.6 | Braun + hem + qtz | In quartz vein |

[a]Braun, braunite; hem, hematite; hol, hollandite; qtz, quartz. All compositions are plotted in Fig. 1 and/or Fig. 4 (for "this paper" no. 8 of Table 1 was chosen)

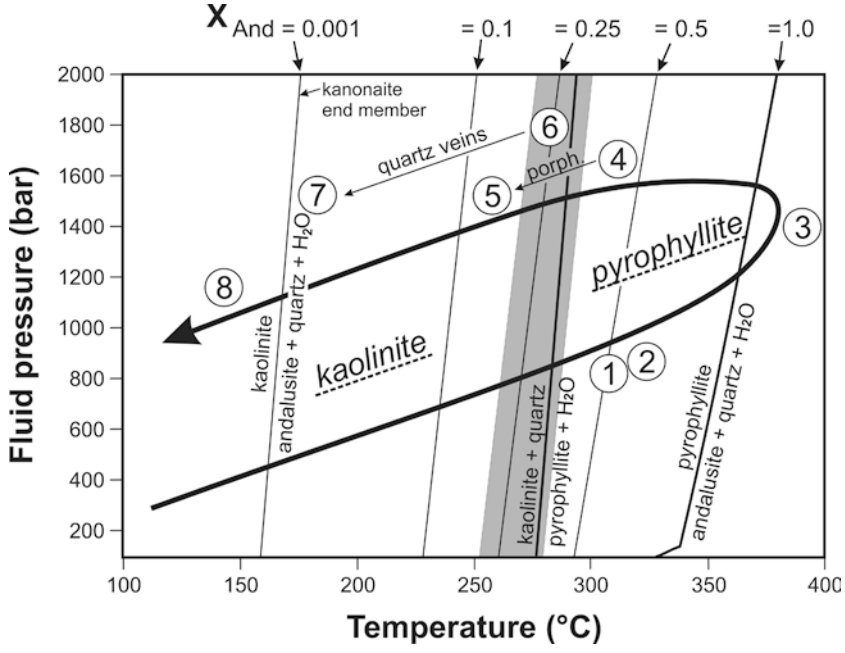


**Fig. 9** Hypothetical pressure–temperature–time path for the phyllites and quartz veins of Le Coreux (*heavy loop* with *arrow*), based on the model of extensional metamorphism as advocated by Fielitz and Mansy (1999). *Heavy* and *light* stability curves refer to mineral reactions in the pure system $Al_2O_3$–$SiO_2$–$H_2O$ as indicated, for water activity = 1. The lower temperature stability limits of the andalusite component are calculated (using the database of Berman 1988; version ba96a.dat) for a series of activities of andalusite taken to equal their molar ratios $X_{And} = Al_2SiO_5/(Al_2SiO_5 + MnAlSiO_5 + FeAlSiO_5)$, as shown in the upper portion (*numbers* accompanying the *light* stability curves). The curve for $X_{And} = 0.001$ is simplified to represent tentatively the lower stability limit of the end-member ferrian kanonaite described here. The *shaded area* represents the range for the low-temperature stability limit of a manganian andalusite with 40 mol% $MnAlSiO_5$ as estimated from experimental data (Abs-Wurmbach et al. 1983a). The *numbers* along the loop represent estimated metamorphic events derived from petrographic observations and analytical data, as listed in Table 7 and further discussed in the text. *Porph.* Development in porphyroblasts

It is thus clear that the changing Mn contents of the Le Coreux andalusite–kanonaite minerals as listed in Table 6 must be explained by varying physical-chemical conditions both in the phyllite and the quartz veins. Because the highest Mn contents appear in the latest growth stages, decreasing temperatures seem to play a significant role. For this possibility, the stability problem of kanonaite now has to be discussed.

The limited experimental results by Abs-Wurmbach et al. (1983a) on the andalusite–kanonaite system are in favour of a prominent influence of low temperatures on kanonaite stability. While for temperatures of 500 °C and more at high oxygen fugacities the limit for maximum solid solution in this system lies near 40 mol% $MnAlSiO_5$, quite independently of pressure, more manganiferous kanonaite could only be crystallized at lower temperatures. The only successful synthesis of a 85-mol% $MnAlSiO_5$–kanonaite was achieved at 400 °C, 2 kbar and very high oxygen fugacity after 50 days (Abs-Wurmbach et al. 1983a, their Table 6 and Fig. 9). Moreover, the lower temperature stability limit for andalusite–kanonaite in the presence of water is shifted to lower temperatures relative to the pure system $Al_2O_3$–$SiO_2$–$H_2O$ (shaded area in Fig. 9).

In summary, it seems that increasing Mn contents stabilize kanonaite to lower and lower temperatures, provided excess (Mn, Fe) minerals coexist at sufficiently high oxygen fugacities. This relationship is used in the next section as the theoretical basis for a petrogenetic model for kanonaite development. Unfortunately, due to the absence of oxygen-buffering mineral pairs, no information can be offered on the magnitude of the prevailing oxygen fugacity, except that it must have been very high. Pulses of oxygen fugacity during vein crystallization may also have been of influence. Abs-Wurmbach and Peters (1999, their Fig. 11) showed that the Mn contents of manganian andalusite increase with rising oxygen fugacity at constant temperature and pressure.

## Petrogenetic model for the development of andalusite–kanonaite minerals at Le Coreux

In this section, a speculative model will be proposed in an attempt to relate the development of the Le Coreux andalusite–kanonaite crystals in their various local environments to the overall changes of the pressure–temperature conditions in the course of regional metamorphism. We do not claim that this is the only possible solution, but at least it is consistent with experimental and theoretical knowledge reported previously, provided local isochemical equilibrium was maintained. Possible open-system behaviour with varying element activities imposed by outside reservoirs, or disequilibrium reactions, will not be discussed here.

**Table 7** Possible petrogenetic events involving andalusite–kanonaite minerals along the hypothetical PTt path of Fig. 9, both in the phyllites and quartz veins of Le Coreux

| Event no.[a] | Porphyroblasts within phyllite | Quartz veins crosscutting the phyllite |
|---|---|---|
| 1–2 | Growth of cores of porphyroblasts with relatively Mn-poor compositions ($X_{And} = 0.5$–$0.6$)[b] | |
| 3 | Growth of pure andalusite ($X_{And} = 1.0$) in Mn-free country rocks | |
| 4–6 | 4–5: development of retrograde zoning in porphyroblasts by continuous reaction to Mn-richer peripheries (kanonaite with $X_{And} = 0.15$), partly leading to zones of kaolinite by hydrous breakdown of Mn-poorer cores | 6: precipitation of kanonaite ($X_{And}$ about 0.25) from fluid together with other Mn minerals (braunite, hollandite) |
| 6–7 | Breakdown of pure andalusite into pseudomorphs with kaolinite | 6–7: continuous reaction of kanonaite with remaining fluids to form peripheral end-member composition ($X_{And} = 0.0$) and remove excess Al by fluids |
| 8 | Partial retrograde breakdown of kanonaite | Partial retrograde breakdown of kanonaite into muscovite + Mn-oxides by reaction with K-bearing fluids |

[a]Numbers are identical to those given in Fig. 9

[b]$X_{And}$ = molar ratio $Al_2SiO_5/(Al_2SiO_5 + MnAlSiO_5 + FeAlSiO_5)$

Kramm (1973) estimated the conditions of the Hercynian metamorphism in the wider region around Le Coreux to 360–380 °C at 1–2 kbar pressure. This is in agreement with the observation that in neighbouring metapelitic rocks pure $Al_2SiO_5$ andalusite had formed as porphyroblasts as well (Theunissen 1970; Fransolet et al. 1977). The question arises, therefore, how the genesis of the Mn, Fe-bearing members of andalusite-group minerals occurring in the Le Coreux mineral locality can be related to that of the more common andalusite-bearing phyllites.

The concept of metamorphism in the Stavelot Massif as part of the entire Ardennes region in the north-western Rhenish Massif has recently been modified by Fielitz and Mansy (1999) by virtue of the suggestion that this metamorphism is caused by an early pre- to synkinematic temperature increase during extension of the Rhenohercynian basin. Such ''extensional'' or ''diastathermal'' metamorphism is typified by anticlockwise pressure–temperature–time (PTt) paths at generally low confining pressures and relatively high temperatures (Robinson and Bevins 1989). A geological environment of this type could probably explain the formation of the typical, formerly andalusite-bearing low-pressure phyllites of regional distribution in the southwest portion of the Stavelot Massif occurring next to the Le Coreux deposit as well.

The tentative petrogenetic model proposed here for the Le Coreux locality assumes such anticlockwise PTt path (Fig. 9), which may provide conditions of high chemical reactivity due to fairly high (water) pressures persisting even under declining temperatures. This reactivity may be necessary for the late developments of the kanonaite phase, and it explains why the pure andalusite porphyroblasts in the neighbouring metapelitic phyllites were nearly completely replaced by kaolinite, so that Kramm (1973) actually considered these pseudomorphs to be primary porphyroblasts of kaolinite.

Because of the paucity of thermodynamic data of highly oxidized Mn-bearing systems, no reliable quantitative derivations of temperature and pressure are possible. Therefore, preliminary calculations of the lower temperature stability limits of members of the andalusite–kanonaite series can solely be based on the simplest possible activity model, in which the chemical activity of $Al_2SiO_5$ equals its molar ratio in the series ($X_{And} = Al_2SiO_5/(Al_2SiO_5 + MnAlSiO_5 + FeAlSiO_5)$). The database of Berman (1988; version ba96a.dat) was used for the calculations. The PT plot of Fig. 9 contains a selection of isopleths, valid only in the presence of excess water, for the andalusite component in the limiting (Mn, Fe) solid solutions, together with the lower stability limit of pure andalusite ($X_{And} = 1.0$) and practically that of end-member kanonaite ($X_{And} = 0.001$) which comes to lie near 160–170 °C. Abs-Wurmbach et al. (1983a, Fig. 6) estimated from experimental data the lower stability limit of an $X_{And} = 0.6$ manganian andalusite to extend near 260–290 °C (shaded area of Fig. 9), which is in loose agreement with the isopleths calculated here. The hydrous Al-silicate formed from the andalusite component at low temperatures is kaolinite below about 270–290 °C, and pyrophyllite between this range and the lower stability limit of andalusite.

The numbers 1–8 along the speculative PTt path of Fig. 9 mark possible events at which mineralogical changes within the phyllites and their crosscutting quartz veins may have occurred. These events are specified in Table 7 based on petrographic observations and analytical data taken from the literature and reported here (Table 6). Additional comments follow below.

The events 1 and 2, interpreted as prograde, are correlated with the analytical data of Kramm (1973, 1979) and would indicate growth of Mn-bearing andalusite phases in the manganiferous phyllite prior to that of pure andalusite, which occurred later in the Mn-free phyllites over large geographic areas (event 3). Therefore, Kramm's (1979, p. 393–394) assumption that occasional layers of kaolinite found within chemically zoned andalusite–kanonaite porphyroblasts of the manganiferous phyllites are pseudomorphous after pure andalusite is difficult to understand. In the present model we consider this kaolinite as evidence for the retrograde continuous hydration reactions of intermediate andalusite–kanonaite to form Mn-richer kanonaite plus kaolinite (events 4–5 following Kramm's (1979) analytical data of the zoned crystals) according to the type equation

$$2(Mn_{0.5}Al_{0.5})AlSiO_5 + SiO_2 + 2H_2O = MnAlSiO_5 + Al_2Si_2O_5(OH)_4,$$

$$\text{manganian andalusite} + \text{quartz} + \text{water} = \text{kanonaite} + \text{kaolinite}.$$

More or less simultaneously, the nearly complete replacement of the pure andalusite porphyroblasts by kaolinite in the regional country rock phyllites (Theunissen 1970; Fransolet et al. 1977) may also have occurred (events 6–7 in Table 7).

Although the time of formation of the discordant quartz veins (event 6) is hard to determine, their andalusite-type phases are restricted to the kanonaite range with Mn contents increasing through time (Schreyer et al. 2001; this paper, Figs. 4 and 5). Therefore, the lowest possible temperatures of stability for these kanonaite compositions calculated are chosen in Fig. 9, knowing that they may also have formed earlier at somewhat higher temperatures. At any rate, similarly as for the phyllite porphyroblasts, continuous reactions of the earliest formed vein kanonaite are assumed (events 6 to 7), which finally led to the end-member ferrian kanonaite described in this paper. Kaolinite was never observed in the quartz veins. Therefore, the mineralising fluid is assumed to have acted as reaction partner.

Final events (8) taking place both in the phyllites and the quartz veins led to the partial peripheral breakdown even of kanonaite (Figs. 2 and 5). Because muscovite appears as a breakdown product, potassium was involved as an additional component. Thus, these reactions may also have taken place already at slightly higher temperatures than shown in Fig. 9, that means within the kanonaite stability field.

**Acknowledgements** Invaluable assistance was given by Olaf Medenbach, Bochum, who removed a kanonaite single crystal from the thin section and prepared it for crystal structure determination. We also thank Thomas Theye, Stuttgart, for detailed thermodynamic discussions, and Michael Burchard, Bochum, who performed the PT calculations of Fig. 9. This paper is dedicated to the late Dr. H.S. Yoder, Jr., former Director of the Geophysical Laboratory, Carnegie Institution of Washington, Washington, D.C., USA, who liked detailed mineral-chemical and crystal-chemical studies on rock-forming minerals when of petrogenetic significance. The paper was materially improved by considering the constructive journal reviews of I. Abs-Wurmbach and Th. Theye.

## References

Abs-Wurmbach I, Peters (1999) The Mn-Al-Si-O system: an experimental study of phase relations applied to parageneses in manganese-rich ores and rocks. Eur J Mineral 11:45–68

Abs-Wurmbach I, Langer K, Seifert F, Tillmanns E (1981) The crystal chemistry of ($Mn^{3+}$, $Fe^{3+}$)-substituted andalusites (viridines and kanonaite), ($Al_{1-x-y}Mn^{3+}{}_xFe^{3+}{}_y)_2$ ($O/SiO_4$): crystal structure refinements, Mössbauer, and polarized optical absorption spectra. Z Kristallogr 155:81–113

Abs-Wurmbach I, Langer K, Schreyer W (1983a) The influence of $Mn^{3+}$ on the stability relations of the $Al_2SiO_5$ polymorphs with special emphasis on manganian andalusites (viridines), ($Al_{1-x}Mn^{3+}{}_x)_2(O/SiO_4)$: an experimental investigation. J Petrol 24:48–75

Abs-Wurmbach I, Peters T, Langer K, Schreyer W (1983b) Phase relations in the system Mn-Si-O: an experimental and petrological study. N Jahrb Mineral Abh 146:258–279

Armbruster T, Gnos E (2000) Tetrahedral vacancies and cation ordering in low-temperature Mn-bearing vesuvianites: indication of a hydrogarnet-like substitution. Am Mineral 85:570–577

Berman RG (1988) Internally consistent thermodynamic data for minerals in the system $Na_2O$-$K_2O$-CaO-MgO-FeO-$Fe_2O_3$-$Al_2O_3$-$SiO_2$-$TiO_2$-$H_2O$-$CO_2$. J Petrol 29:455–522

Burnham CW, Buerger MJ (1961) Refinement of the crystal structure of andalusite. Z Kristallogr 115:269–290

Fielitz W, Mansy J-L (1999) Pre- and synorogenic burial metamorphism in the Ardenne and neighbouring areas (Rhenohercynic zone, central European Variscides). Tectonophysics 309:227–256

Fransolet A-M, Kramm U, Schreyer W (1977) Metamorphose und Magmatismus im Venn-Stavelot-Massiv, Ardennen. Fortsch Mineral 55 Beih 2:75–103

Gunter M, Bloss FD (1982) Andalusite-kanonaite series: lattice and optical parameters. Am Mineral 67:1218–1228

Herbosch A(1968) La viridine et la braunite de Salm-Château. Bull Soc Belg Géol 76:183–205

Hoffmann C, Armbruster T, Kunz M (1997) Structure refinement of (001) disordered gaudefroyite $Ca_4Mn^{3+}{}_3[(BO_3)_3(CO_3)O_3]$: Jahn-Teller-distortion in edge-sharing chains of $Mn^{3+}O_6$ octahedra. Eur J Mineral 9:7–19

Klemm G (1911) Über Viridin, eine Abart des Andalusites. Notizbl Ver Erdk Darmstadt 32:4–13

Kramm U (1973) Chloritoid stability in manganese rich low-grade metamorphic rocks, Venn-Stavelot Massif, Ardennes. Contrib Mineral Petrol 41:179–196

Kramm U (1979) Kanonaite-rich viridines from the Venn-Stavelot Massif, Belgian Ardennes. Contrib Mineral Petrol 69:387–395

Kramm U (1982) Die Metamorphose des Venn-Stavelot-Massivs, nordwestliches Rheinisches Schiefergebirge: Grad, Alter und Ursache. Decheniana (Bonn) 135:121–178

Kulish EA (1961) Manganese-alumina rocks with viridine from the archaean of the Aldan Shield (in Russian). Geol Geofiz Akad Nauk SSSR Sibir Otdel 1:53–65

Piller H (1977) Microscope photometry. Springer, Berlin Heidelberg New York

Ramdohr P (1980) The ore minerals and their intergrowths, 2nd edn, vol 2. Pergamon Press, Oxford

Robinson D, Bevins RE (1989) Diastathermal (extensional) metamorphism at very low grades and possible high grade analogues. Earth Planet Sci Lett 92:81–88

Schreyer W, Fransolet A-M, Bernhardt H-J (2001) Hollandite-strontiomelane solid solutions coexisting with kanonaite and braunite in late quartz veins of the Stavelot Massif, Ardennes, Belgium. Contrib Mineral Petrol 141:560–571

Sheldrick GM (1997) SHELXL-97 program for crystal structure determination. University of Göttingen, Germany

Theunissen K (1970) L'andalousite et ses phases de transformation dans la région de Vielsalm. Ann Soc Géol Belg 93:363–382

Vrána S, Rieder M, Podlaha J (1978) Kanonaite, $(Mn^{3+}_{0.76}Al_{0.23}Fe^{3+}_{0.02})^{[6]}Al^{[5]}[O/SiO_4]$, a new mineral isotypic with andalusite. Contrib Mineral Petrol 66:325–332

Weiss Z, Bailey SW, Rieder M (1981) Refinement of the crystal structure of kanonaite, $(Mn^{3+},Al)^{[6]}(Al,Mn^{3+})^{[5]}O[SiO_4]$. Am Mineral 66:561–567